



Providing Choice & Value

Generic CT and MRI Contrast Agents



CONTACT REP

AJNR

This information is current as of July 28, 2025.

**Dual-Layer Detector Cone-Beam CT
Angiography for Stroke Assessment:
First-in-Human Results (the Next Generation
X-ray Imaging System Trial)**

F. Ståhl, H. Almqvist, J. Kolloch, Å. Aspelin, V. Gontu, E. Hummel, M. van Vlimmeren, M. Simon, A. Thran, Å. Holmberg, M.V. Mazya, M. Söderman and A.F. Delgado

AJNR Am J Neuroradiol published online 13 April 2023
<http://www.ajnr.org/content/early/2023/04/20/ajnr.A7835>

Dual-Layer Detector Cone-Beam CT Angiography for Stroke Assessment: First-in-Human Results (the Next Generation X-ray Imaging System Trial)

 F. Ståhl,  H. Almqvist,  J. Kolloch,  Å. Aspelin,  V. Gontu,  E. Hummel,  M. van Vlimmeren,  M. Simon,  A. Thran,  Å. Holmberg,  M.V. Mazya,  M. Söderman, and  A.F. Delgado



ABSTRACT

BACKGROUND AND PURPOSE: In patients with stroke, IV cone-beam CTA in the angiography suite could be an alternative to CTA to shorten the door-to-thrombectomy time. However, image quality in cone-beam CTA is typically limited by artifacts. This study evaluated a prototype dual-layer detector cone-beam CT angiography versus CTA in patients with stroke.

MATERIALS AND METHODS: A prospective, single-center trial enrolled consecutive patients with ischemic or hemorrhagic stroke on initial CT. Intracranial arterial segment vessel conspicuity and artifact presence were evaluated on dual-layer cone-beam CTA 70-keV virtual monoenergetic images and CTA. Eleven predetermined vessel segments were matched for every patient. Twelve patients were necessary to show noninferiority to CTA. Noninferiority was determined by the exact binomial test; the 1-sided lower performance boundary was prospectively set to 80% (98.75% CI).

RESULTS: Twenty-one patients had matched image sets (mean age, 72 years). After excluding examinations with movement or contrast media injection issues, all readers individually considered dual-layer cone-beam CT angiography noninferior to CTA (CI boundary, 93%, 84%, 80%, respectively) when evaluating arteries relevant in candidates for intracranial thrombectomy. Artifacts were more prevalent compared with CTA. The majority assessment rated each individual segment except M1 as having noninferior conspicuity compared with CTA.

CONCLUSIONS: In a single-center stroke setting, dual-layer detector cone-beam CTA virtual monoenergetic images are noninferior to CTA under certain conditions. Notably, the prototype is hampered by a long scan time and is not capable of contrast media bolus tracking. After excluding examinations with such scan issues, readers considered dual-layer detector cone-beam CTA noninferior to CTA, despite more artifacts.

ABBREVIATIONS: CBCT = cone-beam CT; CBCTA = cone-beam CTA; CNR = contrast-to-noise ratio; DL = dual-layer; VMI = virtual monoenergetic images

Cone-beam CT (CBCT) with flat image detectors was first demonstrated in 2000.¹ The technique is widely used in interventional radiology procedures for anatomic and pathology assessment.²⁻⁵ In patients with stroke, IV CBCT angiography

(CBCTA) in the angiography suite could be an alternative to CTA to shorten the door-to-thrombectomy time.⁶ CBCTA has been shown to be equal or better than CTA for the diagnosis of intracranial stenosis or proximal MCA occlusions.^{7,8} A study in 10 patients indicated superior image-quality results in several CBCTA arterial segments compared with CTA; however, the patient cohort was heterogeneous and biased, and the results were only presented for individual vessel segments.⁹ A retrospective study on 16 patients with stroke with large-vessel occlusion of the anterior circulation indicated that CBCTA generated from a volume perfusion scan can reliably identify the site of occlusion in the ICA and M1 segment of the MCA.¹⁰ However, this study did not find CBCTA superior to CTA.¹⁰


In CTA, virtual monoenergetic images (VMIs) reconstructed from dual-energy scans have superior image quality and improve the diagnostic assessment of intracranial vessels compared with conventional polyenergetic images.¹¹⁻¹³ CBCTA image quality would likely benefit from dual-energy VMI reconstructions by means of

Received October 13, 2022; accepted after revision February 27, 2023.

From the Departments of Neuroradiology (F.S., H.A., J.K., Å.A., V.G., Å.H., M. Söderman, A.F.D.) and Neurology (M.V.M.), Karolinska University Hospital, Stockholm, Sweden; Department of Clinical Neuroscience (F.S., H.A., V.G., M.V.M., M. Söderman, A.F.D.) Karolinska Institutet, Stockholm, Sweden; Image Guided Therapy (E.H., M.v.V.), Phillips Healthcare, Best, the Netherlands; and Philips Research Hamburg (M. Simon, A.T.), Hamburg, Germany.

The trial was supported by a grant from the European Commission (Horizon 2020, NEXIS-project, grant number 780026).

Please address correspondence to Fredrik Ståhl, MD, Department of Neuroradiology, Karolinska University Hospital, Eugeniavaegen 3, 171 76 Stockholm, Sweden; e-mail: Fredrik.stahl@regionstockholm.se

 Indicates open access to non-subscribers at www.ajnr.org

 Indicates article with online supplemental data.

<http://dx.doi.org/10.3174/ajnr.A7835>

reduced beam-hardening artifacts and an improved contrast-to-noise ratio (CNR).^{11–14} Recently, performance characteristics of a prototype dual-layer detector CBCT (DL-CBCT) system were published, with the possibility of optimizing CNR by VMI energy selection.¹⁵

Because previous studies on CBCTA are small, heterogeneous, and selective, a trial enrolling consecutive patients is necessary to determine the role of CBCTA in the primary diagnostic setting of suspected stroke.^{7–10} In this prospective trial, we assessed arterial visibility and artifact presence in patients with stroke when examined with DL-CBCT angiography (DL-CBCTA) and CTA. To our knowledge, this is the first trial on CBCTA with prospectively defined end points, enrolling awake patients with the aim of investigating noninferiority to CTA. Furthermore, this work presents the first-in-human results from a DL-CBCT prototype system.

MATERIALS AND METHODS

Trial Design and Participants

The Next Generation X-ray Imaging System (NEXIS) trial was a prospective, nonrandomized open-label single-sequence, 2-period crossover clinical trial with blinded image readers conducted at a comprehensive stroke center. The study sought to include patients evaluated for endovascular thrombectomy on arrival at the hospital. Patients with a suspected large-vessel occlusion of the anterior circulation underwent prehospital triage to bypass primary stroke centers as per clinical routine.¹⁶ Patients 50 years of age or older with ischemic stroke of the anterior circulation or hemorrhagic stroke were consecutively enrolled from November 2020 to April 2021. Initial imaging was with CTA as per clinical routine and subsequently with the prototype DL-CBCT in an adjacent room. Depending on applicable eligibility criteria, patients were imaged once or twice with DL-CBCT (the same day as CTA or/and 1 day after CTA). Eligibility criteria, inclusion groups, and flow diagrams of study participation are presented in the Online Supplemental Data.

The study protocol and informed consent forms were approved by the Swedish Ethical Review Authority (approval No. 2020–00157). The prototype DL-CBCT system was approved by the Swedish Medical Products Agency (document No. 5.1–2020–6325), in accordance with the Medical Device Directive. Philips Healthcare was the formal sponsor of the study because of direct liability for the prototype DL-CBCT system. An independent qualified research organization contracted by the sponsor monitored the study. All patients signed an informed consent. The trial was supported by a grant from the European Commission (Horizon 2020, NEXIS-project, grant No. 780026). The study was registered prospectively at clinicaltrials.gov (identifier: NCT04571099).

CTA and Prototype DL-CBCTA

The systems used for CTA were Aquilion ONE (Canon Medical Systems) and IQon Spectral CT (Philips Healthcare). The examination was according to clinical routine, typically including noncontrast CT of the head, multiphase CTA, and CTP. The prototype DL-CBCT system (Allura NEXIS Investigational Device; Philips Healthcare) was a commercial interventional C-arm x-ray system (Allura Xper FD20/15; Philips Healthcare) fitted with a dual-layer 20-inch (379.4 × 293.2 mm) non-CE marked detector prototype. The prototype detector has been previously described.¹⁵ In essence,

the dual-layer detector captures more photons than a conventional CBCT detector. DL-CBCTA VMIs were derived from Compton and photoelectric base projections (basis material decomposition was performed in the projection domain). Vessel conspicuity may be improved due to intrinsic compensation of iodine beam-hardening artifacts in DL-CBCTA VMIs. Anticorrelated noise reduction was exploited as an inherent benefit of DL-CBCT.¹⁷ All DL-CBCTA and CTA scans used the same automated injection protocol: 85 mL of iodine, 320 mg I/mL (iodixanol, Visipaque; GE Healthcare), 5 mL/s into a peripheral vein followed by an 80-mL saline chaser.

The second-phase CTA standard reconstruction was included in the study as a reference standard because it was reconstructed with a smaller FOV and the timing was typically more similar to the DL-CBCTA contrast phase (late arterial/arteriovenous). Phantom measurements indicated that the DL-CBCTA and CTA systems had comparable high-contrast spatial resolution. Scan details are shown in Table 1. In conjunction with the CTA and DL-CBCTA, the quality of the image acquisition was evaluated with regard to patient motion and timing of the contrast media injection. Scans were rated as good, acceptable, or poor.

Diagnostic Image-Quality Assessment

A series of pilot studies were performed to determine the optimal VMI energy and noise-reduction levels for the DL-CBCTA images. We randomized 50- to 80-keV VMIs at 3 different noise-reduction levels, and expert readers evaluated them side-by-side blinded to noise and energy levels (F.S., H.A., V.G., M. Söderman, A.F.D.). Window settings were normalized to a previous publication on dual-energy CTA.¹⁸ Images were ranked in order of preference with regard to image quality and artifact presence. The 70-keV images with a moderate noise reduction were best suited for the purpose of the study.

In the reader study, vessel conspicuity and artifact presence were evaluated separately on 5-point Likert scales, adopted with slight modifications from previous studies (5, excellent vessel conspicuity or no artifacts; 1, vessel not visible or extensive artifacts) (see the Online Supplemental Data for a detailed description).^{10,19} All patients had unilateral ischemic or hemorrhagic stroke; thus, the affected hemispheres were not included in the analysis. Images were randomized and evaluated independently by 3 neuroradiologists (H.A., J.K., and Å.A.) each with >9 years of experience in a single-sequence, 2-period crossover design with a mean washout period of 4 weeks (range, 1–8 weeks). The readers were blinded to technique, and there was no clinical information. The study software allowed changes in section thickness, viewing plane, window level, and window width.

Sixteen intracranial arterial segments were prospectively defined for the readers' study. For the powered analysis, some arterial segments were merged to render 11 arterial segments per patient (Table 2). For merged segments, the scores of individually evaluated segments were averaged. The score difference between DL-CBCTA and CTA for each segment in each patient determined whether a segment was considered inferior, equal, or superior. In case of an absent segment due to variant anatomy, a vessel conspicuity score of 1 was given for the specific segment (see the previous paragraph). In addition to individual reader's results, the majority assessment is also presented, ie,

Table 1: Scan details

| | Canon Aquilion ONE | Philips IQon | Prototype DL-CBCT |
|---|-------------------------|----------------------------|----------------------------|
| Tube (kV) | 100 | 120 | 120 |
| Tube current (mAs/mA) (average) | 196 (Auto-modulation) | 114 (Auto-modulation) | 310 |
| Scan time/rotation time (sec) | 3.3/0.5 (Full rotation) | 2.5/0.3 (Full rotation) | 20.0/20.0 (200° rotation) |
| Nominal beam width (mm) | 80 × 0.500 | 64 × 0.625 | 194.700 |
| Pitch factor | 0.813 | 0.671 | NA |
| Display FOV coronal × sagittal × axial (mm ³) | 210.9 × 210.9 × 160.0 | 210.0 × 210.0 × 160.0 | 251.8 × 251.8 × 194.7 |
| Section thickness (mm) | 0.50 | 0.67 | 0.66 |
| Matrix size | 512 × 512 | 512 × 512 | 384 × 384 |
| Reconstruction kernel | FC43 | Filter UA | Ståhl et al ^{15a} |
| Reconstruction algorithm | AIDR 3D eStandard | iDose ⁴ level 4 | Ståhl et al ^{15a} |
| Avg CT DIvol (16-cm phantom) | 20.0 mGy | 21.3 mGy | NA |
| Air kerma (in an 18-cm water phantom) ^b | NA | NA | 57.6 mGy |
| MTF ^c | 50%: 3.78 10%: 6.57 | 50%: 3.46 10%: 6.65 | 50%: 3.57 10%: 6.04 |

Note:—CTDIvol indicates volume CT dose index; MTF, modulation transfer function; NA, not applicable.

^a Details of the prototype algorithm are described in Ståhl et al.¹⁵

^b Air kerma in an 18-cm diameter plastic water phantom at the center of the scan length, measured in accordance with American Association of Physicists in Medicine Task Group Report 111.²⁶

^c Generated from consecutive scans of the upper bead of a Catphan CTP528 module (The Phantom Laboratory).

Table 2: Arterial segments

| 16 Segments | 11 Segments (Powered) | 11 Segments (Thrombectomy) |
|---------------------|-----------------------|----------------------------|
| ICA | ICA | ICA |
| M1 | M1 | M1 |
| M2 | M2 | M2 |
| M3 | M3-M4 | M3 |
| M4 | | M4 |
| A1 | A1-A2 | A1 |
| A2 | | A2 |
| Lenticulostriate | Lenticulostriate | |
| Vertebral | Vertebral | Vertebral |
| Basilar | Basilar | Basilar |
| AICA | AICA-PICA-SCA | |
| PICA | | |
| SCA | | |
| Basilar perforators | Basilar perforators | |
| P1 | P1-P2 | P1 |
| P2 | | P2 |

Note:—Lenticulostriate indicates lenticulostriate artery perforators; Vertebral, intracranial vertebral artery; Basilar perforators, basilar artery perforating branches; SCA, superior cerebellar artery.

segments judged as superior/equal or inferior compared to CTA by at least 2 out of 3 readers.

Statistical Analysis

The powered outcome of this study was the proportion of arterial segments with equal or superior visibility compared with CTA (Table 2). The target proportion was 90% equal or superior ratings, with a lower boundary performance goal set to 80%. The 1-sided α was modified from .025 to .0125, to account for multiple end points. A sample size of 126 was required to render 80% power. Because the powered end point was trait-based, 12 patients with a total of 132 arterial segments (11 segments each) constituted the minimum sample size. For these analyses, the exact binomial test with a 1-sided 98.75% CI was used. Within-subject correlation of arterial segments was assessed by the Cochran-Mantel-Haenszel test.²⁰ Interrater agreement was assessed by the Fleiss κ .²¹ Statistical analyses and graphic presentations were made in R Studio (Version 1.4.1103; <http://rstudio.org/download/desktop>). A biostatistician was consulted at all stages of the study.

RESULTS

Population Characteristics

Of 28 consecutively enrolled patients, 5 had no in-house CTA and 2 underwent subcutaneous IV contrast media injection during the DL-CBCTA scan. Two patients were imaged twice with DL-CBCTA, and for those patients, the results from both scans were averaged. Consequently, 21 complete and matched DL-CBCTA and CTA image sets from 21 patients were included (Fig 1, flow diagram). The mean age was 72 (SD, 9) years, and 14 were women (67%). The right hemisphere was affected in 11 (57%) patients. Three patients had a hemorrhagic stroke. Of the remaining 18 patients with ischemic stroke, 17 (94%) presented with occlusion of the ICA or proximal MCA (M1 or M2 segment) on CTA. Seventeen patients (81%) were imaged with DL-CBCTA the day after CTA imaging (mean, 23.8 [SD, 3.0] hours), of whom 15 had been treated with thrombectomy the day before (modified TICI grade 2C reperfusion or better in 11 [73%]). Because only the unaffected hemisphere was included in the statistical analysis, the degree of reperfusion was not considered to influence the results. Four patients (19%) were only imaged with DL-CBCTA on the same day as CTA (mean, 1.2 [SD, 0.6] hours after CTA).

Vessel Visibility Assessment

For the powered end point of overall arterial visibility, 21 patients with a total of 231 matched arterial segments (11 per patient) were evaluated by each reader. One reader scored equal or superior vessel visibility for DL-CBCTA and CTA in 90% of arterial segments (CI lower boundary of 84%) and met the predefined noninferiority criteria (lower performance boundary of >80%), whereas the other 2 readers did not (CI lower performance boundary of 58% and 53%, respectively). The result of the majority analysis was 77% of arterial segments being rated noninferior in DL-CBCTA (CI lower boundary of 71%). The Fleiss κ between readers was 0.25 (fair agreement). Examples of patient scans with no disagreement among readers and with considerable interrater variability are presented in the Online Supplemental Data.

Post Hoc Subset Analyses

Nine of the 21 (43%) DL-CBCTA scans were of poor quality due to patient motion or suboptimal timing of the contrast media injection (Fig 2). No CTA scan was rated as poor. In a subset analysis including only the 12 matched scans of acceptable or good quality, the 3 readers rated vessel visibility as noninferior in 98%, 88%, and 78% of the cases, respectively, which meant that 2 readers met the predefined performance goal (CI lower boundary of >80%). The majority result for this subset was 98% (CI lower boundary of 93%). See Table 3 for a detailed display of the results.

Eleven arterial segments especially relevant for thrombectomy candidates were selected for evaluation in the same patient subset (Table 2). According to each reader, noninferior vessel visibility was

98%, 91%, and 88%, and all readers individually exceeded the CI lower performance boundary of 80% (Table 3). Majority results were identical to those of the powered subset (98%, CI lower boundary 93%). The Fleiss κ for this data set was 0.38 (fair agreement). There was no significant within-patient correlation of individual arterial segments for any of the individual readers in the thrombectomy data set or subset. However, a significant correlation was found for all majority analyses and most individual reader results for the powered data set and subset (Online Supplemental Data).

Image Artifact Assessment

Image artifacts were assessed in the same arterial segments as used for vessel visibility. For the prospectively determined arterial segments, readers perceived artifact presence as noninferior to CTA in 58%, 42%, and 36% of the segments rated (Table 4). The Fleiss κ was 0.26 (fair agreement). After excluding the 9 scans of inferior quality, noninferiority to CTA for artifact assessment was perceived in 68%, 66%, and 55% of the cases. The lowest number of artifacts compared with CTA was observed in the subset of 11 arterial segments especially relevant for thrombectomy candidates (Table 4). The Fleiss κ for this data set was 0.34 (fair agreement). In summary, noninferiority in terms of artifacts was not seen in the full data set or any subset analysis, given a lower performance boundary of 80%.

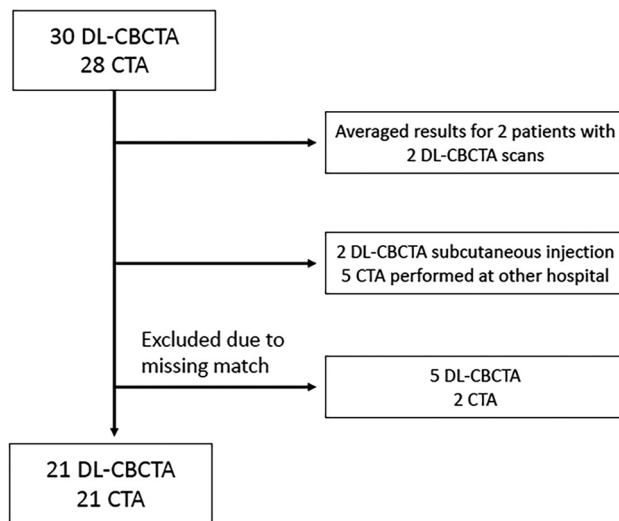


FIG 1. Of 28 consecutively enrolled patients, 5 had no in-house CTA and 2 had subcutaneous IV contrast media injection during the DL-CBCTA scan. Two patients were imaged twice with DL-CBCTA, and for those, the results from both scans were averaged. Consequently, 21 complete and matched DL-CBCTA and CTA image sets from 21 patients were included.

Evaluation of Individual Arterial Segments

The Online Supplemental Data show the whole data set of individual arterial

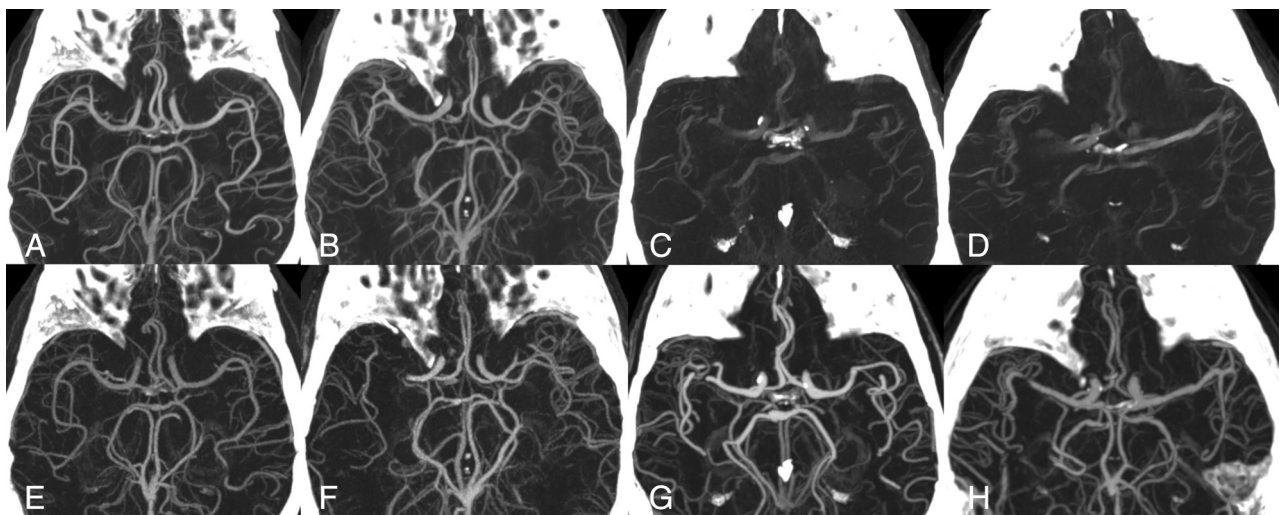


FIG 2. DL-CBCTA 70-keV images (upper row) and CTA (lower row) with MIP 35-mm section thickness. A and B, Acceptable-quality DL-CBCTA scans. C and D, Typical scans in the data set affected by motion artifacts. Lower row (E–H) shows the corresponding CTA. Note that images F, G, and H show a right-sided MCA occlusion, which have been resolved at the time for DL-CBCTA imaging. Only the arterial anatomy in the unaffected hemisphere was evaluated in this study.

Table 3: Vessel visibility^a

| | Powered Data Set | Powered Subset | Thrombectomy Data Set | Thrombectomy Subset |
|----------------|--------------------------|--------------------------|--------------------------|--------------------------|
| Patients | 21 | 12 | 21 | 12 |
| Segments rated | 231 | 132 | 231 | 132 |
| Majority | 0.77 (0.70) | 0.98 (0.93) ^b | 0.77 (0.71) | 0.98 (0.93) ^b |
| Reader 1 | 0.65 (0.58) | 0.88 (0.80) ^b | 0.67 (0.60) | 0.91 (0.84) ^b |
| Reader 2 | 0.90 (0.84) ^b | 0.98 (0.93) ^b | 0.89 (0.83) ^b | 0.98 (0.93) ^b |
| Reader 3 | 0.60 (0.53) | 0.78 (0.69) | 0.68 (0.61) | 0.88 (0.80) ^b |

^a Proportion of DL-CBCTA arterial segment visibility rated equal or superior to CTA. The data set (21 patients) includes all scans; the subset (12 patients) excluded inferior scans. The 98.75% CI of the 1-sided lower performance boundary is in parentheses (lower boundary is defined as 80% rated equal or superior).

^b Statistically significant result.

Table 4: Artifacts^a

| | Powered Data Set | Powered Subset | Thrombectomy Data Set | Thrombectomy Subset |
|----------------|------------------|----------------|-----------------------|---------------------|
| Patients | 21 | 12 | 21 | 12 |
| Segments rated | 231 | 132 | 231 | 132 |
| Majority | 0.41 (0.34) | 0.63 (0.53) | 0.55 (0.48) | 0.81 (0.72) |
| Reader 1 | 0.42 (0.35) | 0.68 (0.58) | 0.54 (0.46) | 0.85 (0.77) |
| Reader 2 | 0.58 (0.50) | 0.66 (0.56) | 0.65 (0.58) | 0.74 (0.64) |
| Reader 3 | 0.36 (0.29) | 0.55 (0.44) | 0.52 (0.44) | 0.73 (0.63) |

^a Proportion of DL-CBCTA arterial segment artifacts rated equal or superior to CTA. Data set (21 patients) includes all scans; subset (12 patients) excluded inferior scans. The 98.75% CI of the 1-sided lower performance boundary is in parentheses (lower boundary is defined as 80% rated equal or superior).

segment ratings per reader and according to the majority assessment. In summary, A2-, M4- and AICA-segment vessel conspicuity was most commonly rated as noninferior to CTA (at least 76% for each reader and segment), with high majority scores (range, 81%–90% rated noninferior). The lenticulostriate and basilar perforating arteries had high majority scores for vessel conspicuity; however, 1 reader's results largely differed from the other 2. It was noted that a safe distinction from small draining veins was difficult. Consequently, the majority score was interpreted with caution for these segments. The A2 segment was rated with the fewest artifacts (majority score, 76% rated noninferior), followed by A1, M2, M3, M4, P1, and P2 segments (majority score, 62%–67%, were rated noninferior).

In the subset of 12 acceptable scans (Online Supplemental Data), A2, M4, AICA, and P2 segments were the most commonly rated as noninferior vessel conspicuity to CTA (at least 92% for each reader and segment). According to the majority assessment, 100% noninferior vessel conspicuity to CTA was seen for all segments except M1 (75% rated noninferior). For artifacts, 100% of A1, A2, M3, M4, and P2 segments were noninferior in the subset according to the majority assessment.

M1-segment vessel conspicuity was noninferior to CTA in 57% of the whole data set and 75% of the subset, the lowest scores registered. The M1 segment also had a higher degree of artifacts (43% rated noninferior in the data set and 67% in the subset). The intracranial ICA segment similarly had a high prevalence of artifacts, and its scores were among the lowest registered.

DISCUSSION

The study compared the intracranial artery visibility of IV DL- CBCTA images with the reference standard CTA in consecutively enrolled patients with stroke. Of dual-detector CBCTA scans, 43% were of poor quality due to movement artifacts or contrast media injection issues. In the subset of patients with acceptable scan quality, DL-CBCTA was noninferior to CTA with regard to intracranial artery conspicuity, despite more prominent image artifacts.

The strengths of the trial were the prospectively defined end points, the clinically relevant study population, and the assessment by blinded readers. The noninferiority lower boundary was set to 80% to minimize the risk of type I error. For the complete data set, 1 reader determined DL-CBCTA arterial visibility as noninferior to CTA, but the other 2 readers did not. However, after excluding DL-CBCTA scans with movement artifacts or suboptimal contrast media injections, 2 readers individually agreed on noninferiority of

DL-CBCTA versus CTA. In this subset, the majority score determined vessel conspicuity to be noninferior to CTA. Image artifacts were generally more abundant in the DL-CBCTA images, and the results did not reach noninferiority.

After we excluded scans of poor quality, all arterial segments except M1 showed noninferior conspicuity to CTA according to the majority assessment. With regard to individual reader results, the M4, A2, P2, and AICA segments had the best vessel visibility in the subset, and all except AICA expectedly indicated a low degree of artifacts in the corresponding segments. The M1 and ICA segments had the lowest scores for vessel visibility compared with CTA and indicated a higher prevalence of artifacts. Our results indicate that arteries that are not influenced by skull base artifacts may have superior conspicuity on DL-CBCTA compared with CTA. As the systems had comparable spatial resolution, this may be attributed to fundamental differences of the VMI (DL-CBCTA) and polyenergetic (CTA) reconstructions. DL-CBCTA VMIs had a lower absolute noise (achieved through anticorrelated noise reduction) and may be superior in mitigating beam-hardening artifacts from iodinated vessels (due to material decomposition in the projection space) compared with CTA. In contrast, arteries adjacent to the skull base showed an inferior visibility compared with CTA. Even though beam-hardening artifacts are mitigated by VMIs, the findings were expected because circular CBCT scans are highly susceptible to skull base artifacts such as beam-hardening.²² Since the M1 and ICA segments are often involved in acute ischemic stroke, future effort should focus on improving visualization of these segments. Recently, a novel x-ray tube trajectory for CBCT was shown to improve intracranial image quality by reducing bone beam-hardening artifacts from the skull.²²

The DL-CBCTA scan time was 20 seconds to enable dual-layer image acquisition. Nine scans (43%) were considered of poor quality, predominantly due to motion artifacts. No repeat scans were performed in this study, in accordance with the ethics approval and study protocol. Most interesting, all except 1 DL-CBCTA scan obtained on the day of admission showed some degree of motion artifacts despite efforts to fixate the head in the head rest. The long scan time is a characteristic disadvantage of CBCT, which must be considered when selecting an appropriate imaging technique for patients with stroke. In awake patients with limited compliance, efforts to minimize the risk of patient movement is warranted. An enhanced head fixation may decrease motion artifacts.²³ Moreover, novel reconstruction methods may mitigate the effects of patient motion in CBCT.^{24,25} If there are still considerable motion artifacts present, one may consider a repeat scan.

Earlier studies evaluating the diagnostic accuracy of CBCTA either had patients under general anesthesia¹⁰ or a highly selective patient cohort able to comply with instructions.⁹ As expected, these studies did not report any significant impact on image quality from motion artifacts. In 1 study, it is unclear whether analyses were matched pair-wise, and the results were presented only for individual vessel segments and not for the CBCTA as a whole.⁹ In addition, outcome measures from previous studies were not prospectively defined and typically were not adjusted for multiple comparisons.⁷⁻¹⁰

This trial has several limitations and technical considerations. The ethics approval did not allow inclusion of patients before treatment. Thus, nonsymptomatic vessel segment conspicuity and artifacts were evaluated as characteristics of diagnostic quality. The original intention was to perform a subset analysis on the diagnostic accuracy to identify intracranial occlusions in a subgroup of patients (inclusion group 3.I, Online Supplemental Data), but the analysis was not performed due to few patients ($n = 3$, of which 2 scans were of poor quality). The study design and power calculation aimed to assess the diagnostic quality of the entire intracranial artery vasculature. In the setting of large-vessel occlusion stroke, it may be favorable to power a diagnostic study with regard to number of patients or only large-diameter arteries, albeit with the risk of missing information about small vessels contributing to collateral flow and small concurrent occlusions.

The results in this study are derived by comparing the same vessel segment in the same patient. Consequently, absent vessel segments due to variant anatomy (for example absent A1 or PICA) received the same vessel conspicuity score in both DL-CBCTA and CTA (ie, 1). However, readers were not specifically instructed on how to assess segments with multiple vessels (lenticulostriate arteries, basilar perforating arteries) or certain variant anatomy (such as an azygos A2 or an AICA-PICA complex). This issue may have increased the interrater variability (κ values were only fair). In the majority results, as well as individual reader results of the powered data set and subset, we show a significant within-patient correlation of arterial segments. In the majority results, this is likely influenced by the M1 segment being most frequently rated inferior. For individual readers, the lenticulostriate arteries and basilar perforators are likely contributors in addition to M1 because they were interpreted inconsistently.

A minority of patients (19%) were imaged with DL-CBCTA shortly after CTA, which may have affected the distribution of iodine contrast media in the DL-CBCTA images. The impact of potential differences in flow dynamics and vessel status for patients imaged with DL-CBCTA 1 day after CTA is unknown. CNR comparison of DL-CBCTA and CTA was not possible because image acquisition timing after IV contrast injections were not identical. A previous study on CBCTA used a 512×512 image pixel matrix, similar to CT.⁹ Using a 384×384 image pixel matrix for DL-CBCTA impacts the level of detail and noise characteristics, possibly affecting the perception of image quality. The DL-CBCTA scan time of 20 seconds made it prone to movement artifacts. Also, in some cases, image quality was poor due to suboptimal timing of the contrast media injection. Because the trial studied a prototype system, manual bolus tracking was not possible. Instead, a manual delay of 15–20 seconds was used for all patients. Furthermore, we used only 1 acquisition protocol. Future studies should involve image acquisition and reconstruction protocol optimization.

DL-CBCTA after IV contrast media injection in angiography suite enables the primary diagnostic work-up and subsequent treatment in the same room. In the clinical setting, this approach would require concurrent image evaluation of the brain to rule out intracranial hemorrhage and to enable assessment of irreversible brain ischemia and possibly brain perfusion. Noncontrast DL-CBCT of the brain has been studied within the scope of the NEXIS trial, and data are currently being prepared for final analysis. Visualization of the cervical vasculature is warranted in patients eligible for thrombectomy; however, this was not addressed in the scope of this study.

CONCLUSIONS

In a single-center stroke setting, DL-CBCTA 70-keV virtual monoenergetic images are noninferior to CTA under certain conditions. Notably, the prototype system is hampered by a long scan time and is not capable of contrast media bolus tracking. After excluding examinations with such scan issues, readers considered DL-CBCTA noninferior to CTA, despite more artifacts.

ACKNOWLEDGMENTS

We thank all members of the NEXIS consortium for a collaborative effort. We thank Kevin Najarian for biostatistics support. We thank Gavin Poludniowski, Artur Omar and Dirk Schäfer for their support in questions regarding medical physics and image reconstruction.

Disclosure forms provided by the authors are available with the full text and PDF of this article at www.ajnr.org.

REFERENCES

1. Jaffray DA, Siewerdsen JH. Cone-beam computed tomography with a flat-panel imager: initial performance characterization. *Med Phys* 2000;27:1311–23 [CrossRef Medline](#)
2. Soderman M, Babic D, Holmin S, et al. Brain imaging with a flat detector C-arm: Technique and clinical interest of XperCT. *Neuroradiology* 2008;50:863–68 [CrossRef Medline](#)
3. Dijkstra ML, Eagleton MJ, Greenberg RK, et al. Intraoperative C-arm cone-beam computed tomography in fenestrated/branched aortic endografting. *J Vasc Surg* 2011;53:583–90 [CrossRef Medline](#)
4. Tacher V, Radaelli A, Lin M, et al. How I do it: cone-beam CT during transarterial chemoembolization for liver cancer. *Radiology* 2015;274:320–34 [CrossRef Medline](#)

5. Doerfler A, Golitz P, Engelhorn T, et al. **Flat-panel computed tomography (DYNA-CT) in neuroradiology: from high-resolution imaging of implants to one-stop-shopping for acute stroke.** *Clin Neuroradiol* 2015;25 Suppl 2:291–97 [CrossRef Medline](#)
6. Brehm A, Tsogkas I, Maier IL, et al. **One-stop management with perfusion for transfer patients with stroke due to a large-vessel occlusion: feasibility and effects on in-hospital times.** *AJNR J Neuroradiol* 2019;40:1330–34 [CrossRef Medline](#)
7. Struffert T, Deuerling-Zheng Y, Kloska S, et al. **Flat detector CT in the evaluation of brain parenchyma, intracranial vasculature, and cerebral blood volume: a pilot study in patients with acute symptoms of cerebral ischemia.** *AJNR Am J Neuroradiol* 2010;31:1462–69 [CrossRef Medline](#)
8. Struffert T, Deuerling-Zheng Y, Kloska S, et al. **Dynamic angiography and perfusion imaging using flat detector CT in the angiography suite: a pilot study in patients with acute middle cerebral artery occlusions.** *AJNR Am J Neuroradiol* 2015;36:1964–70 [CrossRef Medline](#)
9. Saake M, Breuer L, Goelitz P, et al. **Flat detector computed tomography angiography with intravenous contrast application: feasibility for visualization of cerebral arterial vasculature.** *J Neuroimaging* 2013;23:414–20 [CrossRef Medline](#)
10. Hoelter P, Goelitz P, Lang S, et al. **Visualization of large vessel occlusion, clot extent, and collateral supply using volume perfusion flat detector computed tomography in acute patients with stroke.** *Acta Radiol* 2019;60:1504–11 [CrossRef Medline](#)
11. Schneider D, Apfalter P, Sudarski S, et al. **Optimization of kiloelectron volt settings in cerebral and cervical dual-energy CT angiography determined with virtual monoenergetic imaging.** *Acad Radiol* 2014;21:431–36 [CrossRef Medline](#)
12. Leithner D, Mahmoudi S, Wichmann JL, et al. **Evaluation of virtual monoenergetic imaging algorithms for dual-energy carotid and intracerebral CT angiography: effects on image quality, artefacts and diagnostic performance for the detection of stenosis.** *Eur J Radiol* 2018;99:111–17 [CrossRef Medline](#)
13. Neuhaus V, Große Hokamp N, Abdullayev N, et al. **Comparison of virtual monoenergetic and polyenergetic images reconstructed from dual-layer detector CT angiography of the head and neck.** *Eur Radiol* 2018;28:1102–10 [CrossRef Medline](#)
14. Fredenberg E. **Spectral and dual-energy X-ray imaging for medical applications.** *Nuclear Instruments and Methods in Physics Research Section A: Accelerators, Spectrometers, Detectors and Associated Equipment* 2018;878:74–87 [CrossRef](#)
15. Ståhl F, Schäfer D, Omar A, et al. **Performance characterization of a prototype dual-layer cone-beam computed tomography system.** *Med Phys* 2021;48:6740–54 [CrossRef Medline](#)
16. Keselman B, Berglund A, Ahmed N, et al. **The Stockholm Stroke Triage Project: outcomes of endovascular thrombectomy before and after triage implementation.** *Stroke* 2022;53:473–81 [CrossRef Medline](#)
17. Brown KM, Zabic S, Shechter G. **Impact of spectral separation in dual-energy CT with anti-correlated statistical reconstruction.** *Proceedings of the Fully Three-Dimensional Image Reconstruction in Radiology and Nuclear Medicine*, Worcester, Massachusetts. July 2, 2015:491–94
18. Zopfs D, Lennartz S, Abdullayev N, et al. **Generally applicable window settings of low-keV virtual monoenergetic reconstructions in dual-layer CT-angiography of the head and neck.** *Quant Imaging Med Surg* 2021;11:3408–17 [CrossRef Medline](#)
19. Hinkmann FM, Voit HL, Anders K, et al. **Ultra-fast carotid CT-angiography: low versus standard volume contrast material protocol for a 128-slice CT-system.** *Invest Radiol* 2009;44:257–64 [CrossRef Medline](#)
20. Mantel N, Haenszel W. **Statistical aspects of the analysis of data from retrospective studies of disease.** *J Natl Cancer Inst* 1959;22:719–48 [Medline](#)
21. Fleiss JL. **Measuring nominal scale agreement among many raters.** *Psychol Bull* 1971;76:378–82 [CrossRef](#)
22. Cancelliere NM, Hummel E, van Nijmegen F, et al. **The butterfly effect: improving brain cone-beam CT image artifacts for stroke assessment using a novel dual-axis trajectory.** *J Neurointerv Surg* 2023;15:283–87 [CrossRef Medline](#)
23. Leyhe JR, Tsogkas I, Hesse AC, et al. **Latest generation of flat detector CT as a peri-interventional diagnostic tool: a comparative study with multidetector CT.** *J Neurointerv Surg* 2017;9:1253–57 [CrossRef Medline](#)
24. Ouadah S, Jacobson M, Stayman JW, et al. **Correction of patient motion in cone-beam CT using 3D–2D registration.** *Phys Med Biol* 2017;62:8813–31 [CrossRef Medline](#)
25. Li Y, Garrett JW, Li K, et al. **Time-resolved C-arm cone beam CT angiography (TR-CBCTA) imaging from a single short-scan C-arm cone beam CT acquisition with intra-arterial contrast injection.** *Phys Med Biol* 2018;63:075001 [CrossRef Medline](#)
26. American Association of Physicists in Medicine. **Report of American Association of Physicists in Medicine Task Group 111: The Future of CT Dosimetry: Comprehensive Methodology for the Evaluation of Radiation Dose in X-Ray Computed Tomography** (2010). <https://www.aapm.org/pubs/reports/detail.asp?docid=109>. Accessed September 6, 2022